Cell Reports
Physical Science

CellPress
OPEN ACCESS

Article

Balancing crop production and energy harvesting in organic solar-powered greenhouses

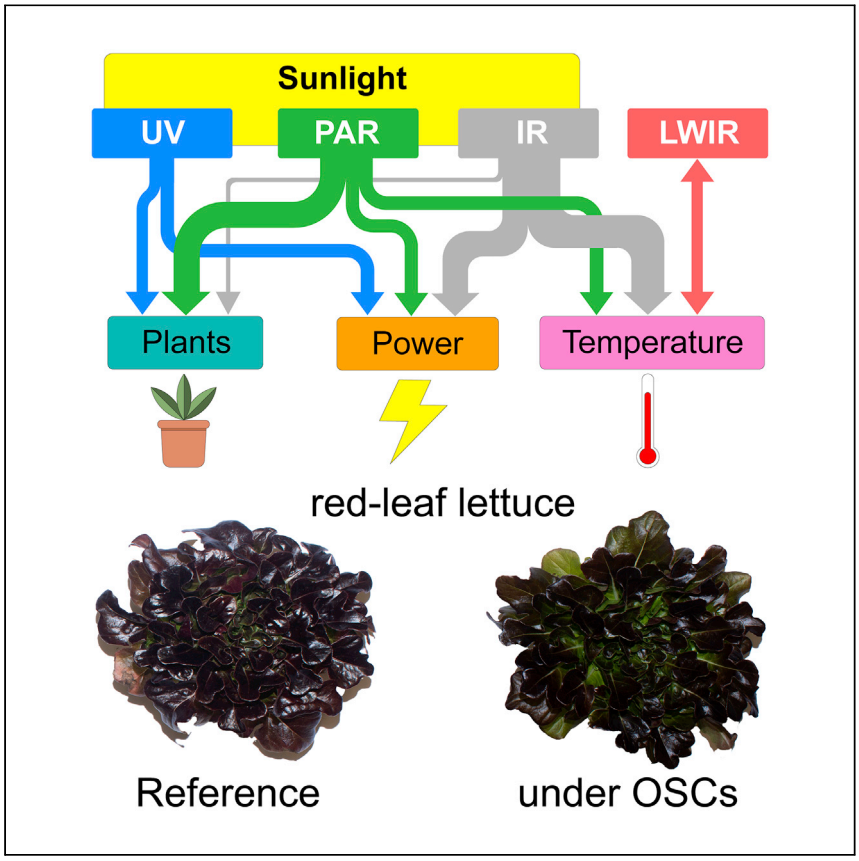

Adding semitransparent organic solar cells (ST-OSCs) to greenhouses can reduce their energy footprint but may also affect plant growth. Ravishankar et al. demonstrate the negligible impact on lettuce grown under ST-OSCs. Furthermore, the trade-offs between solar power, plant growth, and climate control are considered. They show that active layer and electrode selection, along with the use of dielectric Bragg reflectors, provide broad spectral management to fully use the solar spectrum to optimize OSC-integrated greenhouses.

Eshwar Ravishankar, Melodi Charles, Yuan Xiong, ..., Harald Ade, Heike Sederoff, Brendan T. O'Connor

hwade@ncsu.edu (H.A.)
hwsedero@ncsu.edu (H.S.)
btoconno@ncsu.edu (B.T.O.)

HIGHLIGHTS

Lettuce grown under semitransparent organic solar cells show no drop in yield

Nutrient content of lettuce grown under ST-OSCs remain unchanged to control

Several OSCs with unique spectral transmittance result in similar lettuce yield

Adding DBRs to OSCs can increase power generation and improve thermal management

Ravishankar et al., Cell Reports Physical Science 2, 100381
March 24, 2021
https://doi.org/10.1016/j.xcrp.2021.100381

Cell Reports
Physical Science

CellPress
OPEN ACCESS

Article

Balancing crop production and energy harvesting in organic solar-powered greenhouses

Eshwar Ravishankar,[1,7] Melodi Charles,[2,7] Yuan Xiong,[3] Reece Henry,[3] Jennifer Swift,[2] Jeromy Rech,[4] John Calero,[2] Sam Cho,[2] Ronald E. Booth,[1] Taesoo Kim,[6] Alex H. Balzer,[5] Yunpeng Qin,[3] Carr Hoi Yi Ho,[6] Franky So,[6] Natalie Stingelin,[5] Aram Amassian,[6] Carole Saravitz,[2] Wei You,[4] Harald Ade,[3,*] Heike Sederoff,[2,*] and Brendan T. O'Connor[1,8,*]

SUMMARY

Adding semitransparent organic solar cells (ST-OSCs) to a greenhouse structure enables simultaneous plant cultivation and electricity generation, thereby reducing the greenhouse energy demand. However, there is a need to establish the impact of such systems on plant growth and indoor climate and to optimize system tradeoffs. In this work, we consider plant growth under OSCs and system-relevant design. We evaluate the growth of red leaf lettuce under ST-OSC filters and compare the impact of three different OSC active layers that have unique transmittance. We find no significant differences in the fresh weight and chlorophyll content of the lettuce grown under these OSC filters. In addition, OSCs provide an opportunity for further light and thermal management of the greenhouse through device design and optical coatings. The OSCs can thus affect plant growth, power generation, and thermal load of the greenhouse, and this design trade space is reviewed and exemplified.

INTRODUCTION

A greenhouse provides an enclosed environment that allows for crop production in non-native climates and adds more growth cycles per year. The protective environment drastically increases yield while lowering water consumption and pesticide use as compared to conventional farming.[1–3] The transparent envelope is the primary design feature of greenhouses that maximizes sunlight reaching the plants. This insolation also leads to significant space heating that can be beneficial in cold weather, but can result in overheating in warm weather. While the sunlight can support space heating in cold weather, the glazing of the greenhouse has poor thermal insulation, resulting in the greenhouse often requiring heating beyond what the sun can provide. Similarly, the excessive solar gains in summer require cooling approaches such as mechanical ventilation. Hence, the need to thermally regulate a greenhouse, along with the use of supplemental lighting, leads to a large increase in energy consumption compared to conventional farming.[4–6] As a result, the potential for greenhouses to be a form of high-intensity environmentally sustainable agriculture is currently hampered by its external energy demand.

To lower the energy footprint of greenhouses, there has been growing interest in integrating solar cells onto the greenhouse structure, as illustrated in Figure 1.[7–11] In this approach, a portion of light is captured by the solar cells to generate power, while the remaining light transmits into the greenhouse for crop production.

[1]Department of Mechanical and Aerospace Engineering, and Organic and Carbon Electronics Laboratories (ORaCEL), North Carolina State University, Raleigh, NC 27695, USA

[2]Department of Plant and Microbial Biology, North Carolina State University, Raleigh, NC 27607, USA

[3]Department of Physics, and ORaCEL, North Carolina State University, Raleigh, NC 27695, USA

[4]Department of Chemistry, University of North Carolina, Chapel Hill, NC 27514, USA

[5]Department of Chemical and Biomolecular Engineering, Georgia Institute of Technology, Atlanta, GA 30332, USA

[6]Department of Materials Science and Engineering, and ORaCEL, North Carolina State University, Raleigh, NC 27695, USA

[7]These authors contributed equally

[8]Lead contact

*Correspondence: hwade@ncsu.edu (H.A.), hwsedero@ncsu.edu (H.S.), btoconno@ncsu.edu (B.T.O.)

https://doi.org/10.1016/j.xcrp.2021.100381

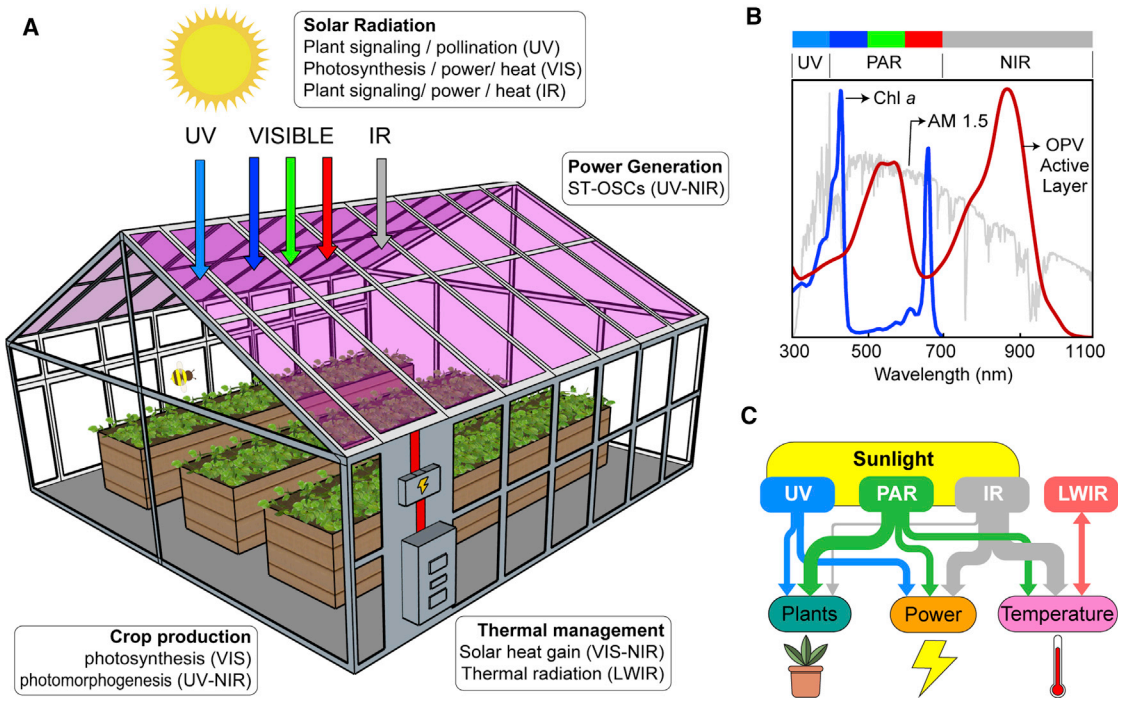

Figure 1. Light utilization in organic solar-power-integrated greenhouses

(A) Overview of an OSC-integrated greenhouse indicating spectral use of sunlight.

(B) Absorption spectra of chlorophyll a (Chl *a*) and active layer of an OSC indicating complimentary absorption.

(C) Schematic flowchart indicating distribution of sunlight toward management of plant growth, electricity generation, and greenhouse temperature management.

Semitransparent organic solar cells (ST-OSCs) have been of particular interest as they have absorption characteristics that can be tuned to complement the spectral light needs of the plant. This potential application also comes at a time of recent advancements in OSC power conversion efficiency, with reports of power conversion efficiency now >18% in opaque, small-area cells.[12–18] Semitransparent OCSs have achieved power conversion efficiencies ranging between 8.1% and 10.2%, with an average visible transmittance (AVT) between 23% and 36%.[18,19] Furthermore, evaporated small-molecule devices with efficiencies of 10.8% and AVTs of 45.7% have also been demonstrated.[18] Recently, we have modeled the energy balance of ST-OSC-integrated greenhouses and showed that net-zero energy systems can be realized in warm and moderate climates with the addition of moderately efficient ST-OSCs on the order of 10%.[20] In colder climates, net-zero energy was not achieved; however, the ST-OSCs continued to provide substantial energy savings. While OSCs provide a beneficial source of power, it is critical that the crops grown in the greenhouse continue to thrive and that there is a net economic benefit to the grower. A recent economic analysis of OSC-integrated greenhouses revealed that while OSCs reduce the environmental impact, compromising crop yield for power generation leads to a steep drop in net present value.[21] This highlights the need to maintain crop yield in solar-integrated greenhouses. Several studies have considered plant growth under solar cells,[7,8,11,22,23] and more specifically under ST-OSCs.[16,24–26] Mung bean sprouts grown under OSCs showed a similar stem length compared to those grown under control conditions.[16] However, this study was conducted over a relatively short period of plant development, and the ability to extrapolate results to actual yields of commercial greenhouse crops is limited. Partial roof coverage with OSCs led to an improved yield of peppers in comparison

to plants grown under control conditions in the same greenhouse.[26] While these results are promising, the OSC roof coverage was limited to ~22% with OSCs that had an average transmittance over the visible spectrum of <14%. In this case, the OSCs largely acted like spectrally neutral shades, and the low coverage limits power generation.[26] Hence, there remains a need to establish the ability to successfully grow greenhouse crops under ST-OSCs with nearly full areal coverage, including the impact of the spectral modification of light on plant development.

In addition to plant productivity, the OSC provides an opportunity to manage light transmittance from the UV to the infrared (IR). In particular, managing light in the IR has significant impacts on the thermal load of the greenhouse. Coatings may be applied that manage near-IR (NIR) solar radiation that contributes significant thermal energy, and coatings that manage long-wavelength (LW) IR that assist in maintaining indoor greenhouse temperatures. Thus, for solar power-integrated greenhouses to be successful, a holistic perspective that takes into account the opportunities and trade-offs between power generation, crop productivity, and greenhouse thermal management is needed, as illustrated in Figure 1.

We evaluated the growth of red leaf lettuce (*Lactuca sativa*) under three distinct ST-OSC filters. Lettuce is selected because it is a commercial greenhouse crop with a large market size.[27] Lettuce also has a reasonably short vegetative period, allowing for multiple replications in a reasonably short period.[28] The OSC filters were composed of high-performance active layers, namely FTAZ:IT-M, FTAZ:$PC_{71}BM$ and PTB7-TH:IEICO-4F,[15,29,30] as shown in Figure S1. The active layers were combined with PEDOT:PSS filters to mimic the optical properties of functional solar cells. These different active layers result in distinct transmission characteristics over the photosynthetically active radiation (PAR) spectrum, which is defined as the wavelength range of light that drives photosynthesis (400–700 nm).[31] This provides a means to assess the role of light intensity and transmission spectra of the OSCs on plant growth and physiology. The studies were conducted in a controlled environment growth chamber that allows for the comparison of plant growth and development under similar illumination, temperature, humidity, CO_2 concentration, and water and nutrient supply. We show that lettuce growth is unhindered under the OSC filters and that the different transmission spectra do not have a statistically significant impact on the fresh weight of the plants. Furthermore, we show that the reduced light intensity reaching the plants reduces the rate of photosynthesis per area, but also increased the leaf area (LA) and leaf number, thereby minimizing the impact on crop yield. The chlorophyll content of the plants is also similar under the different filters. These results demonstrate the possibility of successfully growing certain crops under semitransparent OSCs and highlight that a thorough characterization of crop production is needed to assess crop productivity under ST-OSCs.

While we find that the red leaf lettuce performed well under different OSC filter spectra, lettuce is known to be a low-light-tolerant plant. The ST-OSC and related light requirements may vary depending on the crop selection and climate zone of the greenhouse. To extend and complement the current plant studies, we turn our attention to future design considerations of OSCs for greenhouse applications. The design considerations include light management across the visible and IR spectra. In the visible spectrum, there is an opportunity to tune transmission through OSC active layer selection and inclusion of distributed Bragg reflectors (DBRs). Here, we demonstrate an OSC with an active layer that has absorption characteristics that complement chlorophyll absorption. The OSC performance was also characterized with the addition of DBRs to further manage light and power generation. We

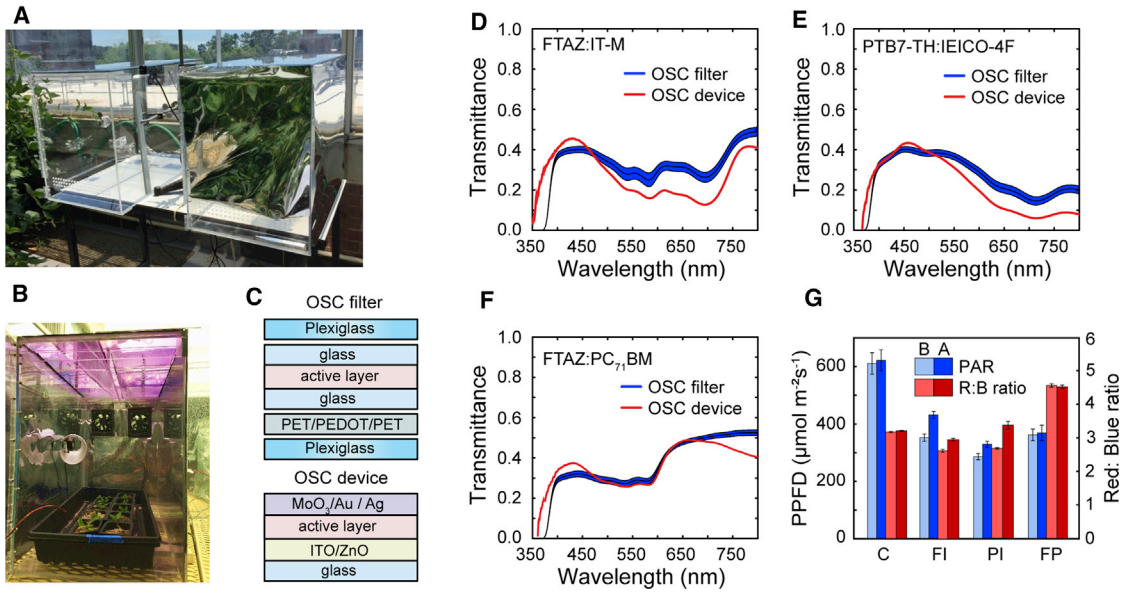

Figure 2. Plant growth experimental setup and the optical properties of the OSC filters

(A) Picture of the growth boxes used for the plant growth study.

(B) Growth box with plant tray covered with OSC filter.

(C) Schematic of the OSC filter and reference ST-OSC device layers.

(D) Transmittance of the OSC filter and ST-OSC device for FTAZ:IT-M.

(E) Transmittance of the OSC filter and ST-OSC device for PTB7-TH:IEICO-4F.

(F) Transmittance of the OSC filter and ST-OSC device for FTAZ:$PC_{71}BM$.

(G) Light flux over PAR (μmol m^{-2} s^{-1}) and red:blue (R:B) ratio at the plant level in round 3 for control (C), FTAZ:ITM (FI), PTB7-TH:IEICO-4F (PI), and FTAZ:$PC_{71}BM$ (FP) treatments, and the flux before the start of the experiments (B) and after the end of the experiment (A).

Data represented as means ± SEMs.

demonstrate a 5%–6% increase in power conversion efficiency with the addition of DBRs designed to reflect green light that is in the absorption gap of chlorophyll or reflect light in the NIR. Thermal management of the greenhouses is also considered by using DBRs to manage NIR and using low emissivity (low-ε) coatings to manage LWIR. We show that increasing the reflection of NIR is beneficial to manage greenhouse temperatures in warm weather, while low-ε coatings reduce the heating demand of the greenhouse in cold weather. The highlighted light-management strategies afforded by the addition of ST-OSCs provides an increased ability to achieve high-productivity, low-environmental-footprint agriculture.

RESULTS AND DISCUSSION

Plant growth experiments

The lettuce seeds were sown in pots that were placed inside growth boxes (21 × 10.5 × 12.5 in) in a large controlled-environment growth chamber (13 × 8 ft), pictured in Figure S2. The box sidewalls were covered in reflective Mylar and the top was covered with OSC filters that ensured that all of the light was transmitted through the filters, as pictured in Figures 2A and 2B. The controlled environment chamber used ceramic metal halide lamps and incandescent lights to mimic sunlight with the spectrum shown in Figure S3A. Four boxes that consisted of the three OSC filters and one control box were placed in the controlled environment chamber for each growth cycle. The OSC filters are non-functioning but were designed to mimic the transmittance of functional ST-OSCs, particularly over the PAR spectrum. The OSC filters consisted of the bulk heterojunction (BHJ) active layer encapsulated between panes of glass followed by a PEDOT:PSS film encapsulated in polyethylene

terephthalate (PET) and all sandwiched between plexiglass, as illustrated in Figure 2C. The control box was covered with glass and two layers of plexiglass. FTAZ:IT-M, FTAZ:$PC_{71}BM$, and PTB7-TH:IEICO-4F were selected as the BHJ layers, with the molecular structure shown in Figure S4. These materials provide a clear difference in transmission over the visible spectrum, as shown in Figures 2D–2F. A comparison of the transmittance of the OSC filters with functional ST-OSCs is also given in Figures 2D–2F, showing reasonably accurate replication. The FTAZ:IT-M, FTAZ:$PC_{71}BM$, and PTB7-TH:IEICO-4F filters have an average transmittance over the PAR spectrum of 29%, 31%, and 38%, respectively. Reference opaque devices with each of the 3 active-layer systems were demonstrated to have a power conversion efficiency of 11%,[30] 6%,[32] and 12%,[15] respectively. Details of the OSCs performance is given in Table S1 and Figure S5. The height of each of the four boxes used in the growth chamber are adjusted to ensure comparable photosynthetic photon flux density (PPFD) at the top of the box. Given differences in transmittance of the OSC filters, this results in differences in the photon flux reaching the plants, as shown in Figure S3B. It is important to note that while the active layer was encapsulated, the transmittance of the OSC filters changed slightly over the course of the experiments, as shown in Figure S6. The change in PAR photon flux and the change in the red (600–700 nm):blue (400–500 nm) light photon flux ratio (R:B) is given in Figure 2G, showing that the color ratio did not change drastically, and the change in PAR flux was <15% over the course of a growth cycle. Further details on filter stability are provided in Note S1. Three replications of the plant growth experiments were carried out, with the PAR photon flux reaching the top of the boxes maintained at ~800 μmol m^{-2} s^{-1} in round 1 (R1) and round 2 (R2) and at ~1,000 μmol m^{-2} s^{-1} in round 3 (R3). Note that 2,000 μmol m^{-2} s^{-1} is equivalent to ~1-sun intensity (1,000 W/m^2). During the experiments, water and nutrient delivery was kept constant between boxes. Harvest was carried out at two stages of the growth cycle. The first stage, called the "transplant stage," was analyzed at 21 days after germination. This denotes a growth phase at which commercial growers often relocate the plants from a germination chamber to greenhouses.[33] The second harvest, called the "final harvest," was analyzed at 35 days after germination, which denotes harvest for market yield. We limit our discussion here to the plant metrics obtained at the final harvest. The transplant stage harvest data are provided in Figures S7–S10).

Crop growth and physiology

The final harvest of lettuce was analyzed for fresh and dry weight, leaf number and size (area), apparent CO_2 fixation rates, stomatal conductivity, and chlorophyll content. An overhead view of a typical lettuce plant at final harvest for each growth condition is pictured in Figure 3A. The fresh and dry weights at final harvest normalized with respect to the control averaged across all three rounds are given in Figures 3B and 3C and the individual round results are given in Figures S11A and S11B. Considering all rounds, the results indicate statistically comparable average fresh weights for lettuce across all OSC filters in comparison to the control treatment. While the average of all of the experimental replications did not show a statistically significant difference in lettuce productivity under the filters compared to the control, there was variation in the overall productivity of lettuce between the three replicates. In R1, the lettuce grown under both PTB7-TH: IEICO-4F and FTAZ:$PC_{71}BM$ filters was found to have statistically lower average fresh weight relative to the control treatment. However, in R2 and R3, these two filter treatments yielded lettuce with fresh weight statistically comparable to the control. The fresh weight of lettuce grown under the FTAZ:ITM filter varied from having fresh weight statistically comparable to the lettuce under control treatment in R1 to having lower fresh weight in R2, and finally higher average fresh weight in R3. The dry weight of the lettuce grown under the

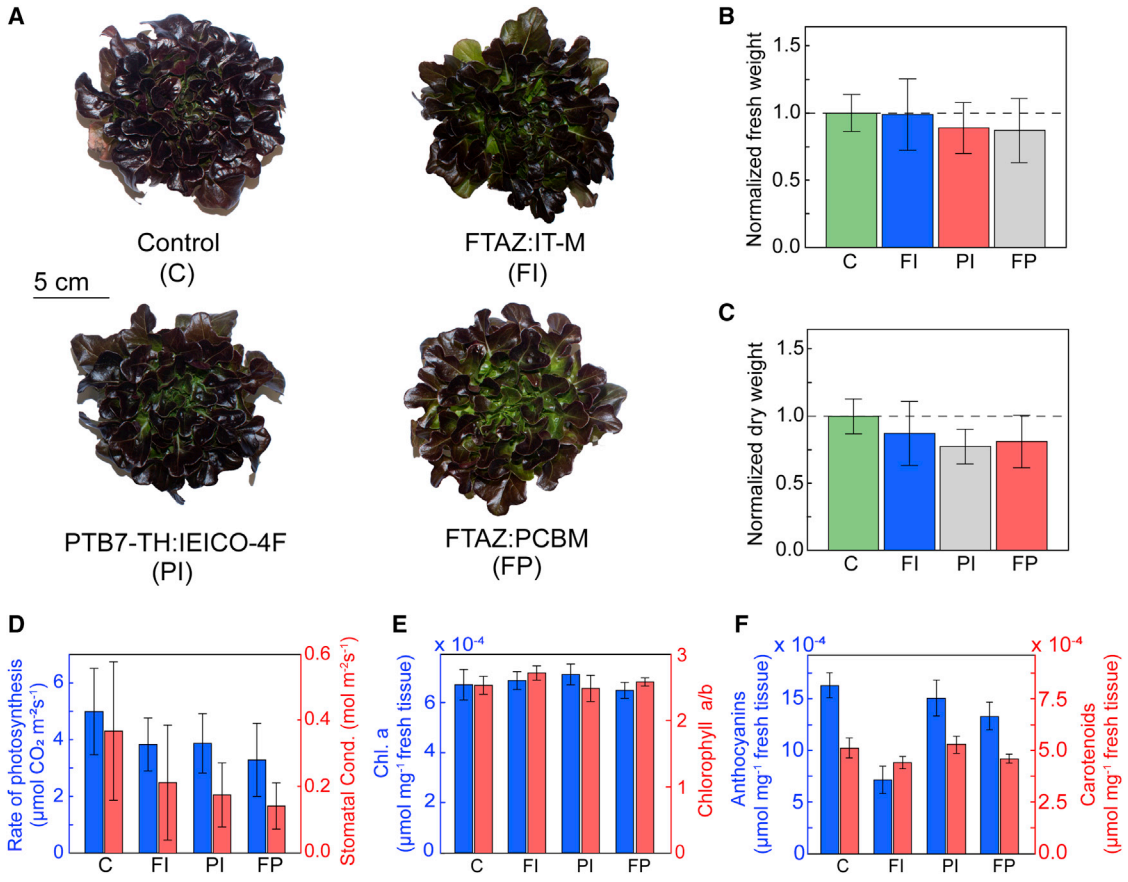

Figure 3. Results of lettuce growth and physiology

(A) Overhead view of lettuce at final harvest for control (C), FTAZ:IT-M (FI), PTB7-TH:IEICO-4F (PI), and FTAZ:$PC_{71}BM$ (FP) treatments.

(B) Normalized fresh weight at final harvest across all replications.

(C) Normalized dry weight at final harvest across all rounds.

(D) Rate of photosynthesis and stomatal conductance at final harvest in round 3.

(E) Chl *a* and chl *a/b* at final harvest in round 3.

(F) Anthocyanin and carotenoid concentration at final harvest in round 3.

Data in (B)–(F) represented as means ± SEMs.

FTAZ:IT-M filter is found to be statistically comparable to the control, while those grown under FTAZ:$PC_{71}BM$ and PTB7-TH:IEICO-4F filter treatments yield lettuce with statistically lower dry weight, with an average drop in dry weight of 18% and 22%, respectively. In comparison, FTAZ:IT-M has an average drop in dry weight of 12%. If only considering R3, which has slightly higher PPFD (1,000 μmol m^{-2} s^{-1} as opposed to 800 μmol m^{-2} s^{-1}in R1 and R2) incident on the growth boxes, the dry weights for all 3 filters are found to be statistically similar to the control (Figure S11). LA and leaf number normalized with respect to the control and averaged across all three rounds are provided for final harvest in Figures S11C and S11D, showing similar behavior for each treatment. Harvest pictures from R2 and R3 are provided in Figures S12 and S13. In summary, although there are some differences across each round, overall, the red leaf lettuce grown under the semi-transparent solar cells has comparable fresh and dry weights to the lettuce grown with the control treatment.

To gain further insight into the plant growth and development, we measured the physiological characteristics of the lettuce, including the rate of photosynthetic

CO_2 fixation; stomatal conductance; and chlorophyll, carotenoid, and anthocyanin concentration. The rate of photosynthetic CO_2 fixation and stomatal conductance as a measure of overall gas exchange between the leaf and the atmospheric environment (CO_2, H_2O, O_2) of the lettuce measured in R3 was observed, with the results provided in Figure 3D. The lettuce grown in the control box was found to have a higher rate of photosynthesis than the lettuce grown under the OSC filters. A similar trend is observed for stomatal conductance. The stomatal conductance is a measure of stomata aperture enabling uptake of CO_2 as well as evaporation of H_2O and controls overall plant performance.[34,35] The total chlorophyll *a* (chl *a*) concentration and the chlorophyll *a/b* (chl *a/b*) ratio in the lettuce is given in Figure 3E and the total chlorophyll *b* (chl *b*) concentration is shown in Figure S14. The chl *a* content and the *a/b* ratio is statistically comparable between lettuce grown under all three OSC treatments with respect to the control. Lastly, the anthocyanin and carotenoid concentration extracted from lettuce in R3 is shown in Figure 3F. These represent a class of antioxidants produced as a measure against damaging light.[36] It is found that except for the FTAZ:IT-M filter treatment, the OSC filters have a statistically comparable anthocyanin concentration to the control, while the carotenoid concentration for all OSC filters are statistically comparable to the control.

Underlying drivers for plant development

The rate of photosynthesis typically shows a curvilinear increase with increasing light intensity up to a light-saturation point.[37,38] Hence, lettuce grown in the control treatment, by virtue of being exposed to higher light intensity, has a higher rate of photosynthesis as compared to the lettuce grown under the OSC filters. However, the lettuce grown under all of the OSC filter treatments have average fresh weights that are statistically comparable to the control. This is in part due to an increase in LA. This behavior is likely due to a shade response by the lettuce, thereby aiding light interception and thus increasing CO_2 fixation. An increase in LA is attributed to a higher partitioning of the assimilated CO_2 into the leaves.[39,40] Across all of the replications, lettuce grown under the FTAZ:IT-M treatment have an average LA that is ~15% higher than the control (Figure S11). FTAZ:IT-M had the lowest transmittance among the three OSC filters in the PAR region and is correlated with the filter treatment resulting in the greatest LA.

When comparing the lettuce grown under the three OSC filters, the spectral differences in the filters can be considered by splitting the spectra transmitted by the filters into the R:B ratio. The R:B ratios ranged from 2.5 (PTB7-TH:IEICO-4F) to 4.5 (FTAZ:PC_{71}BM), as shown in Figure 2G. Wang et al.[41] observed that stomatal conductance and rate of photosynthesis are driven in part by the R:B ratio. With a decrease in the R:B ratio, an increase in the rate of photosynthesis and stomatal conductance was observed.[42] However, here, lettuce growing under the three OSC filters had a statistically similar rate of photosynthesis and all were lower than the control. This indicates that the differences in R:B ratio were not large enough to drive differences in the rate of photosynthetic CO_2 fixations.

In vascular plants, chl *a* and chl *b* are the red and blue light-absorbing pigments in the light-harvesting complexes of the photosystems. The absorption spectra of chl *a* and chl *b* differ slightly and the ratio of chl *a/b* is responsive to light intensity.[43,44] A higher ratio of chl *a/b* indicates a high light-adapted photosynthetic apparatus, indicating a higher capacity for electron transport.[41] This has the potential to increase light absorption, which in turn is beneficial for CO_2 fixation. Figure 3E, however, indicates that chl *a/b* is found to be statistically comparable between lettuce grown under all three OSC treatments with respect to the control. It is notable

that a similar chlorophyll content was found for all lettuce growth conditions, despite the control having nearly 40%–50% higher light intensity than that found under the OSC stacks. This behavior is consistent with previous studies in which Wang et al.[41] reported no significant change in chl *a/b* for lettuce treated under light having R:B in the range of 1–4. Furthermore, lettuce grown under shaded conditions relative to the control have been known to possess higher total chlorophyll content per unit fresh weight, which provides further reasoning to the comparable chlorophyll content observed between the control and the three OSC filters.[45,46] Finally, by visual inspection (Figure 3A), it is apparent that the red coloration is strongest for lettuce grown as part of the control. This suggests differences in anthocyanin content, which are pigments responsible for the red coloration. This is clearly indicated in Figure 3F, where we see a higher mean anthocyanin concentration for lettuce grown as part of the control treatment. While anthocyanin production is associated with several environmental stresses, including light intensity, it also acts as a source of antioxidants.[47] The higher anthocyanin content in the control is likely due to the higher light intensity incident on the lettuce. Despite lower PPFD at the plant level, we find that the FTAZ:$PC_{71}BM$ treatment results in statistically comparable anthocyanin concentration. For the carotenoid concentration, we see no statistically significant difference between control and the three OSC filter treatments.

To conclude, we find that the lettuce adapted to the changing lighting conditions to maintain similar yield and thereby show minimal adverse impact on crop growth due to OSC filter integration. Furthermore, the spectral changes between the OSC filters were not large enough to drive significant differences in lettuce development. While lettuce grown under control conditions with higher light intensities contained more of the nutritionally desirable antioxidant anthocyanin as compared to the FIAZ:IT-M and PTB7-TH:IEICO-4F filter treatment, this limitation will likely not occur at the higher overall light intensities in a greenhouse setting or can be alleviated by the induction of anthocyanin biosynthesis by other means of abiotic stress.

Organic solar cell design outlook

The lighting demands in the greenhouse will depend on geographic location and crop. While the lettuce is shown to grow well under the ST-OSCs, it is known to be a shade-tolerant crop.[7] For plants that have greater lighting demands, alternative ST-OSC device designs and active layers may be needed. The greenhouse location will also dictate the daily solar radiation entering the greenhouse as well as the heating and cooling needs of the space. In this section, we consider ST-OSC design considerations that affect crop production, electricity generation, and the thermal load of the facility.

A primary means to manage the transmission of the ST-OSC across the PAR spectrum is through material selection of the active layer. In addition to photosynthetic light absorption by chlorophyll, plants use the wavelength composition and direction of light as spatiotemporal clues to adjust and adapt their growth and development, referred to as photomorphogenesis.[42] Thus, the exact spectral needs will likely depend on the plant under consideration. Here, we demonstrate the ability to tune the absorption of the ST-OSC to complement the absorption spectrum of chlorophyll. The ST-OSC is composed of a ternary active layer of FTAZ:IEICO-4F:$PC_{71}BM$.[48–50] The transmittance of the ST-OSC is shown in Figure 4A, showing transmittance peaks that correspond with the absorption of chl *a*, which is centered at 400 and 650 nm. The current voltage characteristics of the OSC are given in Figure 4B, with the performance metric summarized in Table 1. While further device optimization is possible, this example clearly demonstrates how active layer material

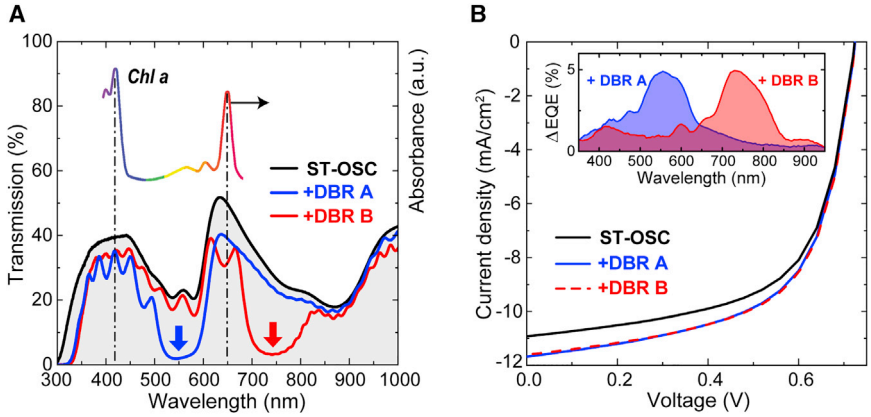

Figure 4. Device characteristics of ST-OSC device with and without DBR coatings

(A) Transmission spectra of semi-transparent OSC and the same device combined with DBR-A and DBR-B. Inset is the absorbance of chl *a*.

(B) Current density-voltage characteristics of the ST-OSC along with the ST-OSC with DBR-A and DBR-B. Inset, change in external quantum efficiency (ΔEQE) of the ST-OSC with the addition of DBR-A and DBR-B.

selection can be used to manage light transmission across the PAR spectrum. Contemporary optimization of materials and devices have focused on optimizing the power conversion efficiency (PCE) in opaque devices or color-neutral ST-OCSs. There should be considerable room for further improvements in ST-OSC performance that account for the spectral needs of greenhouses, particularly with the use of the very recent development of high-performing donor polymer D18, which has nearly an identical absorption spectrum to FTAZ.[51]

As part of the OSC design, there is an opportunity to add DBRs that manage light in the visible and NIR spectra.[52,53] By managing reflection in the visible region, there is the opportunity to reflect selective portions of the spectrum that are not efficiently used by the plant to then be absorbed by the solar cell for increased power generation. As an example, we experimentally demonstrate the use of solution-processed DBRs that consist of alternating layers of a titanium oxide hydrate:poly(vinyl alcohol) hybrid material and poly(methyl methacrylate) (PMMA). Two DBRs were considered, with DBR-A having a stopband centered at 560 nm and DBR-B having a stopband centered at 745 nm, with transmittance shown in Figure S15. The transmission of the ST-OSC combined with DBR-A and -B is shown in Figure 4A, while the current voltage characteristics of the ST-OSC with the DBRs are shown in Figure 4B. The addition of the DBRs increases reflection in the region of the DBR stopband, thereby resulting in a 5% and 6% increase in short-circuit current density with DBR-A and DBR-B, respectively. The summary of ST-OSC performance with the DBRs is provided in Table 1. The enhancement in external quantum efficiency (ΔEQE) is shown in Figure 4B, demonstrating that the increase in EQE corresponds with the

Table 1. Summary of ST-OSC device characteristics with and without DBR-A and DBR-B

DBR	J_{SC} (mA/cm^2)	V_{OC} (V)	FF (%)	PCE (%)	ΔJ_{SC} (%)	ΔPCE (%)
Without	10.92	0.723	62.11	4.90	–	–
A	11.68	0.724	60.94	5.16	6.96	5.3
B	11.60	0.725	61.75	5.19	6.23	5.9

The performance metrics include the short-circuit current density (J_{SC}), open-circuit voltage (V_{OC}), fill factor (FF), and power conversion efficiency (PCE). The enhancement in current density (ΔJsc) and efficiency (ΔPCE) with the DBR coatings are also included.

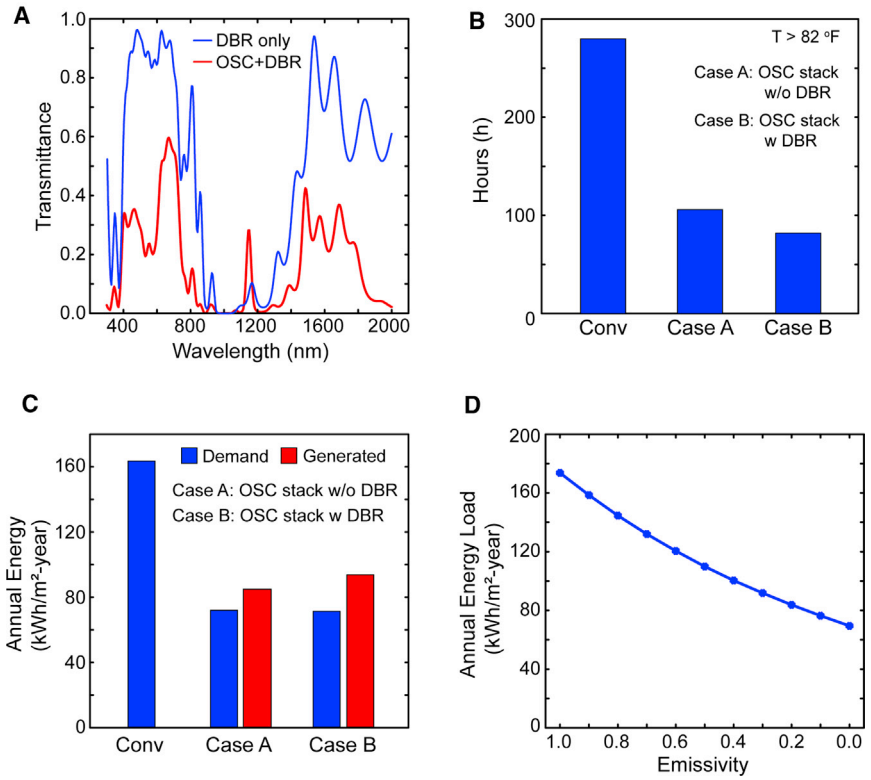

Figure 5. Modeled ST-OSC device with optimized DBR stack for maximizing NIR reflection

(A) Transmittance of DBR coating and DBR coating with ST-OSC.

(B) Number of hours in a year the greenhouse exceeds its setpoint temperature.

(C) Annual energy demand and solar power generation for a greenhouse in Sacramento, California for (i) conventional greenhouse, (ii) greenhouse with rooftop ST-OSC, and (iii) greenhouse with rooftop ST-OSC and DBR coating.

(D) Annual energy load for a greenhouse in Sacramento, California as a function of emissivity of the greenhouse envelope.

stopbands of the DBRs. The ST-OSC stack without any DBR stopband has a PAR transmittance of 36%. This reduces to 27% with the DBR-A stopband and 32% with DBR-B stopband.

Finally, light management in the IR ranging from NIR ($\lambda > 700$ nm–2 μm) to LWIR ($\lambda >$ 8 μm) will have a direct impact on the energy demand needed to manage the temperature inside the greenhouse. The NIR sunlight contains ~50% of the total solar energy, resulting in significant heating potential. The LWIR is relevant for managing thermal radiation near room temperature, where blackbody radiation of an object at 22°C (295 K) has a peak in intensity at a wavelength of 9.8 μm. By minimizing the emissivity of the glazing to the environment (i.e., increasing LWIR reflection), thermal radiation from within the greenhouse is reflected, helping to maintain the temperature inside the greenhouse.

The use of DBRs with reflection in the NIR can improve OSC power generation for active layers that absorb in this spectral range, as shown with the DBR-B design (Figure 4B). For greenhouses in warm climates, the use of DBRs in the NIR will also result in lowering the thermal gains and support better greenhouse temperature management in summer. To examine this impact, we consider rooftop OSCs that integrate DBR coatings with high transmission across the PAR spectrum and high reflection

from 800 to 1,600 nm. The transmittance of the OSC stack and the standalone DBR coating is provided in Figure 5A. Change in PAR transmittance as a result of DBR integration was maintained to be <1% in comparison to a ST-OSC system without DBRs. Details of the DBR layer thickness and number of layers for reflection in the IR is provided in the experimental procedures. The simulated ST-OSC stack with the integrated DBRs is found to possess a heat rejection rate of 90% over a wavelength region of 700–2,000 nm. This heat rejection rate coupled with PAR transmittance and PCE were found to be comparable to recently reported ST-OSC devices with similar DBR design.[52–54] We then modeled the energy load of a greenhouse in Sacramento, California following a previously described greenhouse energy model.[20] This location was chosen because California represents the largest greenhouse market in the United States.[55] We found that the addition of the DBR with NIR reflection results in only a minor decrease in the energy consumption used for cooling. This is due to the greenhouse using low-energy-consuming fan-pad evaporative cooling, as typically found in a semi-closed greenhouse.[56] However, there is a clear improvement in the ability to maintain the temperature within the greenhouse structure as shown in Figure 5B. The number of hours in 1 year that the temperature in the greenhouse cannot be maintained below the temperature setpoint used to grow tomatoes of 82°F (27.8°C) reduces from 280 h for a conventional greenhouse to 82 h for a ST-OSC-integrated greenhouse with the DBR coating added to the OSC stack. This is despite the conventional greenhouse using shade cloths with 50% transmittance in summer to manage heat. While not covered here, maintaining the greenhouse temperature setpoint results in significant improvements in plant health and should be considered in optimizing the system.[57]

Figure 5C shows the annual energy demand and solar power generation for each of the simulated greenhouse cases discussed here when using the FTAZ:IEICO-4F:$PC_{71}BM$ active layer. We see that the ST-OSC integrated greenhouse without DBR achieves net-zero energy demand for annual operation. Adding the NIR-reflecting DBR coating to the OSC stack improves power generation by 10%, resulting in an increase in surplus energy of the system. The increased power generation is due to the increased reflection in the spectral region that is absorbed by IEICO-4F. Note that the energy demand decreases when adding the OSC to the greenhouse structure, which is largely attributed to the low-ε of the indium tin oxide (ITO) electrode, discussed further below. While the results show immense promise, it is important to remember that NIR light management will be highly dependent on the location of the greenhouse. The DBRs provide better temperature control in summer, but the greater NIR reflection may lead to greater heating demand in winter, particularly in colder climates. Thus, the use of DBR coatings to manage light over the visible and NIR spectra will be dependent on the crop, the energy demands of the greenhouse, and its geographical location.

LWIR is typically managed in glazings through low-ε coatings that are often thin metal and metal oxide films. ITO and silver (Ag) have low emissivity and are commonly used in ST-OSCs providing inherent LWIR management.[58–60] As shown in Figure 5D, adding the OSCs to the roof of the greenhouse reduces its energy demand largely due to the use of Ag with an emissivity of 0.1,[58] reducing the heating demand in winter. The impact of LWIR emissivity of the greenhouse glazing on the annual energy load is shown in Figure 5D. We find that as the emissivity of the greenhouse roof drops from 1.0 to 0.1, there is a 67% reduction in the heating demand of the greenhouse. These results highlight that not only can the OSC be used to generate power but it can also be used to manage IR light that can have significant effects on the power generation and heating and cooling demand of a greenhouse.

Integrating ST-OSCs onto greenhouse structures provides an opportunity to generate power, lowering the external energy demands of a greenhouse. The OSC design will also affect the plant development and the heating and cooling load of the greenhouse space. The present article highlights the needs for a holistic viewpoint and the trade space between plant production, power generation, and thermal load to assess the opportunity of ST-OSC greenhouse integration. The potential impact of using ST-OSCs in greenhouses on plant production was considered by looking at the growth of red leaf lettuce grown under three spectrally unique OSC filters. We demonstrated that ST-OSCs can be used for the successful cultivation of lettuce without a major impact on yield and plant health. We found that there is a decrease in the photosynthetic rate for the lettuce grown under the filters due to a decrease in photon flux, but this is compensated for by an increase in LA, resulting in similar biomass for each OSC filter considered relative to the control. Interestingly, we found that the lettuce yield was similar irrespective of the OSC filter, demonstrating flexibility in material selection for this crop. For practical implementation, scale up of the semitransparent solar modules will still be necessary. In this implementation, the areal coverage and transmittance of the modules will differ from the experimental conditions, possible allowing for increased natural light incident on the plant. These results thus suggest that large-scale implementation will maintain positive outcomes. While lettuce proved to be a successful demonstration, this may not translate to other crops that have different lighting needs. We thus considered how OSC active layer material selection can be used to manage spectral transmission characteristics. A ternary OSC consisting of a FTAZ:IEICO-4F:$PC_{71}BM$ blend that has a transmission profile with peaks that match well with the absorption spectra of chlorophyll was demonstrated. The transmission was then further managed with the addition of DBRs that reflect light outside the chlorophyll absorption spectrum and increase the power generation of the solar cell.

The use of DBR coatings not only provides an opportunity to increase power generation but it also can be used to reduce overheating in the greenhouse. We show that for a greenhouse in Sacramento, California, the number of hours that the greenhouse overheats can be reduced from 280 to 82 h when using OSCs with a DBR tuned to reflect NIR light. While this does not have a large impact on energy demand, it is expected to improve crop production. Lastly, using OSC electrodes that can also function as low-ε coatings was shown to significantly reduce the heating load of the greenhouse. Combining the minimal impact observed on plant productivity, along with power generation and improved thermal management with the use of ST-OSC, suggest that integrating OSCs with greenhouses is a promising strategy to achieve environmentally sustainable high-intensity greenhouse-based agriculture.

EXPERIMENTAL PROCEDURES

Resource availability

Lead contact

Further information and requests for resources and reagents should be directed to and will be fulfilled by the lead contact, Brendan T. O'Connor (btoconno@ncsu.edu).

Materials availability

This study did not generate new unique reagents.

Data and code availability

The published article and associated Supplemental information includes all of the necessary data required for evaluating the main findings of this study. Any additional data related to this study are available from the lead contact upon request.

Plant growth experiment

Lettuce seeds were germinated and grown in pots inside growth boxes of the dimensions 21 × 10.5 × 1.25 in. Each pot was filled with 50% Sunshine Redi-Earth Pro growing mix and 50% pea gravel. The growth boxes were then planted in a controlled environment growth chamber that was 13 × 8 ft. Each growth box was equipped with temperature, humidity, and CO_2 sensors that logged data every 5 min. The lighting and growth boxes positions in the environmental chamber were adjusted to ensure that a similar intensity of light was incident on the top of each box. Given the differences in the transmittance of the filters, the light intensity incident on the plants in R3 ranged from 611 μmol m^{-2} s^{-1} (29 mol m^{-2} day^{-1}) for the control to 285 μmol m^{-2} s^{-1} (13 mol m^{-2} day^{-1}) for FTAZ:IT-M. Plants under FTAZ:PC_{71}BM filter and PTB7-TH:IEICO-4F filter have a daylight integral of 17 mol m^{-2} day^{-1}. To regulate the temperature inside the box, each box housed two constant speed fans. Seeds were germinated directly in the boxes and initially four seeds were placed in each pot. Watering is done by hand until germination. After germination, the plants are thinned to two per pot. At this stage, water and nutrients are fed automatically through pipes that lead to each box from a central system and controlled remotely to evenly distribute to the plants. Across each round, the chamber was regulated to have a photoperiod of 13/11 h (light/dark), temperature of 21°C/19°C (day/night), and a CO_2 concentration of 450 μmol mol^{-1}. To compensate for positional light variance, the pots are rotated within each box on alternate days. Harvest was carried out at two stages of the growth cycle, with the transplant stage being 21 days after germination and the final harvest stage being 35 days after germination. At each stage, four plants were harvested for analysis.

Biomass, LA, rate of photosynthesis, and stomatal conductance

Measurements of fresh weight, dry weight, LA, and leaf number were made on four plants in each OSC filter treatment and control. Three replicate studies of the plant growth were carried out. Dry weight was measured by heating the leaves of the harvested plant for 3 days at 65°C. Both fresh and dry weight does not include root mass in the calculation. LA was measured using a LI-COR LI-3000. The rate of photosynthesis and stomatal conductance were measured with a LI-COR 6400XT portable photosynthesis system. All of the measurements were collected from plants inside the growth boxes while under light. Survey measurements were collected using an extended reach chamber from two leaves of approximately the same age for four plants per treatment. Data collection took place in the 5 days before the final harvest and ended within 5 h of the beginning of the light period each day. Ambient CO_2 conditions were maintained inside the chamber with soda lime scrubbers.

Secondary metabolite extraction

Secondary metabolites were extracted and quantified following a modification of the protocols previously described.[61] Two to three mature leaves were collected from four plants per treatment and flash frozen in liquid nitrogen. Tissue was ground in liquid nitrogen, weighed, and suspended in either chlorophyll and carotenoid extraction buffer or anthocyanin extraction buffer. Absorption was measured in triplicate with a Biotek Synergy HT microplate reader and Gen5 software with pathlength correction. The absorption wavelengths and metabolite concentration equations were used as previously described. Concentrations were reported per milligram of fresh weight.

ST-OSC filter preparation for plant experiments

The solution and coating parameters of the polymer and small molecule of the three active layer material systems used for the plant growth experiment are shown in

Table S2. The solution was heated to 80°C overnight and then wire bar coated onto 20 × 10 cm glass substrates. Ethylene vinyl acetate (EVA) films are then adhered along the edge of a cover glass used for encapsulations. The EVA strips are adhered by heating to 110°C–120°C. The cover glass was then laminated onto the active layer coated glass and heated using a hot plate at 100°C to ensure the seal under a nitrogen atmosphere. Optical epoxy (Norland 63) was then coated around the edge of the filter stack and cured under 365 nm UV light for 20 min to form a secondary seal. Twelve filters combined to cover one growth box. Similarly, PEDOT:PSS (PH1000, Hareaus) was wire bar coated onto a PET substrate and then laminated under another layer of PET.

Fabrication of reference ST-OSC devices

ST-OSC devices were fabricated on transparent ITO-coated glass substrates using an inverted device configuration (glass/ITO/ZnO/active layer/MoO_3/Au/Ag). After cleaning the ITO glass, a ~30-nm-thick so-gel ZnO was spin coated on the substrate and annealed at 150°C for 30 min in ambient air. The active layers were spin coated in a nitrogen atmosphere. The FTAZ:IT-M films was coated from a toluene solution consisting of FTAZ:IT-M 1:1 wt ratio at a total concentration of 10 mg/mL, resulting in a 70-nm-thick film. The film was then thermally annealed at 150°C for 10 min. The FTAZ:PC_{71}BM film was coated from a trichlorobenzene solution consisting of FTAZ:PC_{71}BM 1:2 wt ratio and a total concentration of 18 mg/mL, resulting in a 60-nm-thick film. The PTB7-TH:IEICO-4F film was coated from a chlorobenzene solution with 3% 1-chloronaphthalene with PTB7-TH:IEICO-4F 1:1.5 wt ratio and a total solvent concentration of 25 mg/mL, resulting in a 118-nm film. The semi-transparent solar cells were completed by the thermal evaporation of 10 nm MoO_3/1 nm Au/10 nm Ag at a pressure of ~1×10^{-6} mbar through a shadow mask.

Semi-transparent FTAZ:IEICO-4F:PC_{71}BM ternary device

The device architecture considered was glass/ITO/ZnO/active layer/MoO_3/Au/Ag/MoO_3/LiF. The FTAZ:IEICO-4F:PC_{71}BM (1:1:0.3 wt ratio) dissolved in a 23-mg mL^{-1} toluene:chloronaphthalene (99:1 volume ratio) solution was spin coated at 2,000 rpm for 60 s to obtain a film thickness of ~100 nm. The electrode consisted of MoO_3/Au/Ag/MoO_3/LiF deposited by vacuum thermal evaporation. The first MoO_3 layer (10 nm) was deposited as a hole transporting layer, followed by Au (0.5 nm) as a wetting layer and Ag (8 nm) as an anode layer. Finally, a capping layer of MoO_3 (20 nm) and an anti-reflective layer of LiF (60 nm) were deposited. The active area of the solar cells was 6.9 mm^2, as defined by the overlap of bottom and top electrodes.

DBR preparation and characterization

The DBRs for this study were produced with alternating layers of a titanium oxide hydrate:poly(vinyl alcohol) (PVAl) hybrid material[62] and PMMA. A total of 8.5 bilayers were dip coated on the front and back of the glass substrates, with the first and last layer on each side produced from the hybrid material. The hybrid acts as the high refractive index layer, n_{600nm} = 1.83, and the PMMA as the low refractive index layer, n_{600nm} = 1.49.

Titanium oxide hydrate solutions were prepared by the hydrolysis of $TiCl_4$ to a final concentration of 0.5 M titanium. Hybrid titanium oxide hydrate:PVAl solutions were prepared by introducing corresponding amounts of the produced titanium oxide hydrate solution to a 40-g/L aqueous solution of PVAl while stirring at room temperature to achieve a 60 vol% titanium oxide hydrate concentration with respect to PVAl.[63,64] Multi-layer samples were fabricated by dip coating of glass substrates in

air at ambient temperature. Due to the crosslinking of the hybrid films during drying, alternation of dipping in hybrid solutions (formulated from 0.5 M titanium oxide hydrate solutions and 40 g/L PVA aqueous solution) and PMMA solution in toluene (4 wt% PMMA) was possible. Withdrawal speeds varied between 5 and 15 mm/min to achieve the desired thicknesses. Between each layer, samples were left to dry vertically inside the fume hood for at least 20 min before the next layer was applied. In total, 8.5 bilayers of hybrid material and PMMA (i.e., 9 layers of hybrid material and 8 layers of PMMA) were cast on both sides of the glass, beginning and ending with the hybrid layers. A final annealing step was performed after the produced DBRs were stored in a desiccator for 7 days. Annealing was carried out at 150°C in an oven for 5 min in air and atmospheric pressure.

The transmittance of multilayer structures was measured at normal incidence using a double-beam Agilent Cary 5000 UV-Vis-NIR spectrophotometer. Refractive indices and thicknesses of the hybrid and PMMA films were calculated using the Fresnel coefficient form of the transfer matrix method.[63] The 60 vol% hybrid refractive index is $n = 1.75 + 0.029/\lambda^2$, and the PMMA refractive index is $n = 1.48 + 0.005/\lambda^2$, where λ is the wavelength in microns.

Solar cell characterization

Current voltage characteristics were recorded with a Keithley 2400 source meter under 100 mW cm^{-2} AM 1.5 G light. The light is provided by a Class 3A Solar Simulator and KG5 silicon reference cell. EQE measurements were conducted using an in-house setup consisting of a DC xenon arc lamp light source, an ORIEL 74125 monochromator, an SR570 current amplifier, and an SR830 DSP lock-in amplifier. An aperture was used to ensure that only the active area was illuminated by the monochromatic beam. Where used, the DBR was placed on the transparent top electrode of the ST-OSC when the current voltage, EQE, and transmittance were measured.

Modeling high IR reflection DBR

Using alternating layers of a titanium oxide hydrate:PVAl hybrid material and PMMA, an IR-DBR stack capable of reflecting over a wavelength range of 800–1,600 nm is modeled. The thickness and the total number of DBR bilayers are modified to achieve the necessary target transmittance profile through a gradual evolution method combined with a needle optimization technique.[65,66] The transmittance of the DBR stack is shown in Figure 5A. Optimization was done to ensure the minimal drop in transmittance in PAR. However, to account for any reduction in PAR, a pair of LiF and MoO_3 optimized to maximize transmittance across PAR is added to the IR-DBR stack. This is then added to the ST-OSC device with FTAZ:IEICO-4F:$PC_{71}BM$ as the active layer following a device architecture described previously. The modeled device architecture is shown in Figure S16. The simulated electric field intensity (|E|2) as a function of thickness of the OSC device stack is provided in Figure S17 for a wavelength in the PAR and IR region to illustrate DBR function.

Modeling greenhouse energy consumption

A 29.4 × 7.3 m single-span gable-roof greenhouse with a gutter height of 3 m is considered. The greenhouse is oriented north to south with a roof tilt angle of 27°. Excluding the north-facing wall, which is considered an opaque surface as it often interfaces with other buildings, all of the surfaces are made up of a 4-mm single-pane glass. Ventilation is provided by fans coupled with evaporative cooling pads, while heating is provided by a combination of forced hot air furnace and a radiant roof heating system. The temperature setpoint for the greenhouse is set between 60°F and 65°F at night and between 70°F and 82°F during the day. A 50%

transmittance neutral shade cloth is considered during the daytime in summer for conventional greenhouses as part of heat management. For modeling OSC stack, we consider the same device architecture used for the fabrication of the ST-OSC system with FTAZ:IEICO-4F:$PC_{71}BM$ as the active layer. Further details on ST-OSC modeling, including the transmittance of light into the greenhouse, are provided by Ravishankar et al.[20]

SUPPLEMENTAL INFORMATION

Supplemental information can be found online at https://doi.org/10.1016/j.xcrp.2021.100381.

ACKNOWLEDGMENTS

E.R., M.C., Y.X., R.H., J.S., J.R., J.C., S.C., R.E.B., Y.Q., C.S., W.Y., H.A., H.S., and B.T.O. acknowledge the NSF INFEWS award 1639429 for support of this research. T.K. and A.A. were supported by ONR grant N00014-20-1-2183 and NCSU start-up funds; A.H.B. and N.S. were supported by NSF award 1905901; C.H.Y.H. and F.S. were supported by NextGen Nano Limited, ONR grant N00014-17-1-2242, and ONR grant N00014-17-1-2204.

AUTHOR CONTRIBUTIONS

H.A., B.T.O., and H.S. provided the conceptual framework and directed the study. E.R., M.C., J.S., and J.C. performed the plant growth experiments, with input from H.S. and C.S. S.C. fabricated the growth boxes, and E.R. set up the fans and sensors in the boxes. M.C. and J.C. performed the Li-COR measurements. M.C. extracted the carotenoid and anthocyanin concentrations. Y.X. and R.H. fabricated the OSC filter stack used for the plant growth experiment. J.R. and W.Y. provided the polymer semiconductors for filter fabrication. R.E.B., T.K., Y.Q., and C.H.Y.H. fabricated and tested the semitransparent OSCs with input from A.A., H.A., B.T.O., and F.S. A.H.B. and N.S. designed, fabricated, and characterized the DBR stacks. E.R. performed the greenhouse energy modeling with input from B.T.O. and H.A. E.R. drafted the initial manuscripts versions, followed by editing and interpretation from all of the co-authors.

DECLARATION OF INTERESTS

The authors declare no competing interests.

Received: November 18, 2020
Revised: February 1, 2021
Accepted: February 24, 2021
Published: March 17, 2021

REFERENCES

1. Ramankutty, N., Evan, A.T., Monfreda, C., and Foley, J.A. (2008). Farming the planet: 1. Geographic distribution of global agricultural lands in the year 2000. Global Biogeochem. Cycles *22*, https://doi.org/10.1029/2007GB002952.

2. Vos, R., Bellù, L.G., Stamoulis, K., and Haight, B. (2017). The Future of Food and Agriculture – Trends and Challenges (Food and Agriculture Organization of the United Nations).

3. Cook, R., and Calvin, L. (2005). Greenhouse Tomatoes Change the Dynamics of the North American Fresh Tomato Industry. https://www.ers.usda.gov/publications/pub-details/?pubid=45477.

4. Bot, G., Van De Braak, N., Challa, H., Hemming, S., Rieswijk, T., Straten, G.V., and Verlodt, I. (2005). The solar greenhouse: state of the art in energy saving and sustainable energy supply. Acta Hortic. *691*, 501–508.

5. Barbosa, G.L., Gadelha, F.D., Kublik, N., Proctor, A., Reichelm, L., Weissinger, E., Wohlleb, G.M., and Halden, R.U. (2015). Comparison of land, water, and energy requirements of lettuce grown using hydroponic vs. conventional agricultural methods. Int. J. Environ. Res. Public Health *12*, 6879–6891.

6. Nadal, A., Llorach-Massana, P., Cuerva, E., López-Capel, E., Montero, J.I., Josa, A., Rieradevall, J., and Royapoor, M. (2017). Building-integrated rooftop greenhouses: an energy and environmental assessment in the Mediterranean context. Appl. Energy *187*, 338–351.

7. Allardyce, C.S., Fankhauser, C., Zakeeruddin, S.M., Grätzel, M., and Dyson, P.J. (2017). The influence of greenhouse-integrated photovoltaics on crop production. Sol. Energy *155*, 517–522.

8. Cossu, M., Murgia, L., Ledda, L., Deligios, P.A., Sirigu, A., Chessa, F., and Pazzona, A. (2014). Solar radiation distribution inside a greenhouse with south-oriented photovoltaic roofs and effects on crop productivity. Appl. Energy *133*, 89–100.

9. Yano, A., Kadowaki, M., Furue, A., Tamaki, N., Tanaka, T., Hiraki, E., Kato, Y., Ishizu, F., and Noda, S. (2010). Shading and electrical features of a photovoltaic array mounted inside the roof of an east-west oriented greenhouse. Biosyst. Eng. *106*, 367–377.

10. Yano, A., Onoe, M., and Nakata, J. (2014). Prototype semi-transparent photovoltaic modules for greenhouse roof applications. Biosyst. Eng. *122*, 62–73.

11. Kadowaki, M., Yano, A., Ishizu, F., Tanaka, T., and Noda, S. (2012). Effects of greenhouse photovoltaic array shading on Welsh onion growth. Biosyst. Eng. *111*, 290–297.

12. Yan, C., Barlow, S., Wang, Z., Yan, H., Jen, A.K.Y., Marder, S.R., and Zhan, X. (2018). Non-fullerene acceptors for organic solar cells. Nat. Rev. Mater. *3*, 1–19.

13. Cui, Y., Yao, H., Zhang, J., Zhang, T., Wang, Y., Hong, L., Xian, K., Xu, B., Zhang, S., Peng, J., et al. (2019). Over 16% efficiency organic photovoltaic cells enabled by a chlorinated acceptor with increased open-circuit voltages. Nat. Commun. *10*, 2515.

14. Zhao, J., Li, Y., Yang, G., Jiang, K., Lin, H., Ade, H., Ma, W., and Yan, H. (2016). Efficient organic solar cells processed from hydrocarbon solvents. Nat. Energy *1*, 15027.

15. Song, X., Gasparini, N., Ye, L., Yao, H., Hou, J., Ade, H., and Baran, D. (2018). Controlling Blend Morphology for Ultrahigh Current Density in Nonfullerene Acceptor-Based Organic Solar Cells. ACS Energy Lett. *3*, 669–676.

16. Liu, Y., Cheng, P., Li, T., Wang, R., Li, Y., Chang, S.Y., Zhu, Y., Cheng, H.W., Wei, K.H., Zhan, X., et al. (2019). Unraveling Sunlight by Transparent Organic Semiconductors toward Photovoltaic and Photosynthesis. ACS Nano *13*, 1071–1077.

17. Cui, Y., Yao, H., Zhang, J., Xian, K., Zhang, T., Hong, L., Wang, Y., Xu, Y., Ma, K., An, C., et al. (2020). Single-Junction Organic Photovoltaic Cells with Approaching 18% Efficiency. Adv. Mater. *32*, e1908205.

18. Xiong, Y., Booth, R.E., Kim, T., Ye, L., Liu, Y., Dong, Q., Zhang, M., So, F., Zhu, Y., Amassian, A., et al. (2020). Novel Bimodal Silver Nanowire Network as Top Electrodes for Reproducible and High-Efficiency Semitransparent Organic Photovoltaics. Sol. RRL *4*, 1–9.

19. Jiang, B.H., Lee, H.E., Lu, J.H., Tsai, T.H., Shieh, T.S., Jeng, R.J., and Chen, C.P. (2020). High-Performance Semitransparent Organic Photovoltaics Featuring a Surface Phase-Matched Transmission-Enhancing Ag/ITO Electrode. ACS Appl. Mater. Interfaces *12*, 39496–39504.

20. Ravishankar, E., Booth, R.E., Saravitz, C., Sederoff, H., Ade, H.W., and O'Connor, B.T. (2020). Achieving Net Zero Energy Greenhouses by Integrating Semitransparent Organic Solar Cells. Joule *4*, 490–506.

21. Hollingsworth, J.A., Ravishankar, E., O'Connor, B., Johnson, J.X., and DeCarolis, J.F. (2020). Environmental and economic impacts of solar-powered integrated greenhouses. J. Ind. Ecol. *24*, 234–247.

22. Loik, M.E., Carter, S.A., Alers, G., Wade, C.E., Shugar, D., Corrado, C., Jokerst, D., and Kitayama, C. (2017). Wavelength-Selective Solar Photovoltaic Systems: Powering Greenhouses for Plant Growth at the Food-Energy-Water Nexus. Earths Future *5*, 1044–1053.

23. Thompson, E.P., Bombelli, E.L., Shubham, S., Watson, H., Everard, A., D'Ardes, V., Schievano, A., Bocchi, S., Zand, N., Howe, C.J., et al. (2020). Tinted Semi-Transparent Solar Panels Allow Concurrent Production of Crops and Electricity on the Same Cropland. Adv. Energy Mater. *10*, 2001189.

24. Emmott, C.J.M., Röhr, J.A., Campoy-Quiles, M., Kirchartz, T., Urbina, A., Ekins-Daukes, N.J., and Nelson, J. (2015). Organic photovoltaic greenhouses: a unique application for semi-transparent PV? Energy Environ. Sci. *8*, 1317–1328.

25. Okada, K., Yehia, I., Teitel, M., and Kacira, M. (2018). Crop production and energy generation in a greenhouse integrated with semi-transparent organic photovoltaic film. Acta Hortic. *1227*, 231–239.

26. Zisis, C., Pechlivani, E.M., Tsimikli, S., Mekeridis, E., Laskarakis, A., and Logothetidis, S. (2020). Organic photovoltaics on greenhouse rooftops: effects on plant growth. Mater. Today Proc. *21*, 65–72.

27. Fu, W., Li, P., and Wu, Y. (2012). Effects of different light intensities on chlorophyll fluorescence characteristics and yield in lettuce. Sci. Hortic. (Amsterdam) *135*, 45–51.

28. Sublett, W.L., Barickman, T.C., and Sams, C.E. (2018). The effect of environment and nutrients on hydroponic lettuce yield, quality, and phytonutrients. Horticulturae *4*, 48–62.

29. Bauer, N., Zhang, Q., Zhao, J., Ye, L., Kim, J.H., Constantinou, I., Yan, L., So, F., Ade, H., Yan, H., et al. (2017). Comparing non-fullerene acceptors with fullerene in polymer solar cells: a case study with FTAZ and PyCNTAZ. J. Mater. Chem. A Mater. Energy Sustain. *5*, 4886–4893.

30. Ye, L., Xiong, Y., Zhang, Q., Li, S., Wang, C., Jiang, Z., Hou, J., You, W., and Ade, H. (2018). Surpassing 10% Efficiency Benchmark for Nonfullerene Organic Solar Cells by Scalable Coating in Air from Single Nonhalogenated Solvent. Adv. Mater. *30*, 1705485.

31. McCree, K.J. (1971). The action spectrum, absorptance and quantum yield of photosynthesis in crop plants. Agric. Meteorol. *9*, 191–216.

32. Lin, Y., Zhao, F., Prasad, S.K.K., Chen, J.-D., Cai, W., Zhang, Q., Chen, K., Wu, Y., Ma, W., Gao, F., et al. (2018). Balanced Partnership between Donor and Acceptor Components in Nonfullerene Organic Solar Cells with >12% Efficiency. Adv. Mater. *30*, e1706363.

33. Spalholz, H., Perkins-Veazie, P., and Hernández, R. (2020). Impact of sun-simulated white light and varied blue:red spectrums on the growth, morphology, development, and phytochemical content of green- and red-leaf lettuce at different growth stages. Sci. Hortic. (Amsterdam) *264*, 109195.

34. Kinoshita, T., Doi, M., Suetsugu, N., Kagawa, T., Wada, M., and Shimazaki, K. (2001). Phot1 and phot2 mediate blue light regulation of stomatal opening. Nature *414*, 656–660.

35. Zhen, S., and Bugbee, B. (2020). Steady-state stomatal responses of C 3 and C 4 species to blue light fraction: interactions with CO 2 concentration. Plant Cell Environ. *43*, 3020–3032.

36. Lester, G.E. (2006). Environmental regulation of human health nutrients (ascorbic acid, β-carotene, and folk acid) in fruits and vegetables. HortScience *41*, 59–64.

37. Goudriaan, J., and van Laar, H.H. (1994). Modelling Potential Crop Growth Processes (Springer Science & Business Media).

38. Yamori, W., Evans, J.R., and Von Caemmerer, S. (2010). Effects of growth and measurement light intensities on temperature dependence of CO(2) assimilation rate in tobacco leaves. Plant Cell Environ. *33*, 332–343.

39. Gommers, C.M.M., Visser, E.J.W., St Onge, K.R., Voesenek, L.A.C.J., and Pierik, R. (2013). Shade tolerance: when growing tall is not an option. Trends Plant Sci. *18*, 65–71.

40. Folta, K.M., and Childers, K.S. (2008). Light as a growth regulator: controlling plant biology with narrow-bandwidth solid-state lighting systems. HortScience *43*, 1957–1964.

41. Wang, J., Lu, W., Tong, Y., and Yang, Q. (2016). Leaf morphology, photosynthetic performance, chlorophyll fluorescence, stomatal development of lettuce (Lactuca sativa L.) exposed to different ratios of red light to blue light. Front. Plant Sci. *7*, 250.

42. Briggs, W.R., and Olney, M.A. (2001). Photoreceptors in plant photomorphogenesis to date. Five phytochromes, two cryptochromes, one phototropin, and one superchrome. Plant Physiol. *125*, 85–88.

43. Larsson, U.K., Anderson, J.M., and Andersson, B. (1987). Variations in the relative content of the peripheral and inner light-harvesting chlorophyll a b-protein complex (LHC II) subpopulations during thylakoid light adaptation and development. Biochim Biophys Acta Bioenerg. *894*, 69–75.

44. Galvão, V.C., and Fankhauser, C. (2015). Sensing the light environment in plants: photoreceptors and early signaling steps. Curr. Opin. Neurobiol. *34*, 46–53.

45. Ilić, Z.S., and Fallik, E. (2017). Light quality manipulation improves vegetable quality at harvest and postharvest: A review. Environ. Exp. Bot. *139*, 79–90.

46. Beneragama, C., and Goto, K. (2011). Chlorophyll *a*:*b* Ratio Increases Under Low-Light in "Shade-tolerant" *Euglena gracilis*. Trop. Agric. Res. *22*, 12–25.

47. Zhang, Y., Xu, S., Cheng, Y., Peng, Z., and Han, J. (2018). Transcriptome profiling of anthocyanin-related genes reveals effects of light intensity on anthocyanin biosynthesis in red leaf lettuce. PeerJ *6*, e4607.

48. Cui, Y., Yang, C., Yao, H., Zhu, J., Wang, Y., Jia, G., Gao, F., and Hou, J. (2017). Efficient Semitransparent Organic Solar Cells with Tunable Color enabled by an Ultralow-Bandgap Nonfullerene Acceptor. Adv. Mater. *29*, 1703080.

49. Schubert, S., Meiss, J., Müller-Meskamp, L., and Leo, K. (2013). Improvement of transparent metal top electrodes for organic solar cells by introducing a high surface energy seed layer. Adv. Energy Mater. *3*, 438–443.

50. Kim, T., Gao, Y., Hu, H., Yan, B., Ning, Z., Jagadamma, L.K., Zhao, K., Kirmani, A.R., Eid, J., Adachi, M.M., et al. (2015). Hybrid tandem solar cells with depleted-heterojunction quantum dot and polymer bulk heterojunction subcells. Nano Energy *17*, 196–205.

51. Liu, Q., Jiang, Y., Jin, K., Qin, J., Xu, J., Li, W., Xiong, J., Liu, J., Xiao, Z., Sun, K., et al. (2020). 18% efficiency organic solar cells. Sci. Bull. (Beijing) *65*, 272–275.

52. Cao, Y., Shi, H., Liu, X., Sun, C., Yao, H., Xia, R., Yip, H.-L., Hou, J., and Huang, F. (2018). Heat-Insulating Multifunctional Semitransparent Polymer Solar Cells. Joule *2*, 1816–1826.

53. Wang, D., Qin, R., Zhou, G., Li, X., Xia, R., Li, Y., Zhan, L., Zhu, H., Lu, X., Yip, H.L., et al. (2020). High-Performance Semitransparent Organic Solar Cells with Excellent Infrared Reflection and See-Through Functions. Adv. Mater. *32*, e2001621.

54. Li, X., Xia, R., Yan, K., Yip, H.L., Chen, H., and Li, C.Z. (2020). Multifunctional semitransparent organic solar cells with excellent infrared photon rejection. Chin. Chem. Lett. *31*, 1608–1611.

55. Cook, R., and Calvin, L. (2005). North American Greenhouse Tomatoes Emerge as a Major Market Force. https://www.ers.usda.gov/amber-waves/2005/april/north-american-greenhouse-tomatoes-emerge-as-a-major-market-force/.

56. Sabeh, N.C., Giacomelli, G.A., and Kubota, C. (2006). Water use for pad and fan evaporative cooling of a greenhouse in a semi-arid climate. Acta Hortic. (719), 409–416.

57. Thompson, H.C., Langhans, R.W., Both, A.J., and Albright, L.D. (1998). Shoot and root temperature effects on lettuce growth in a floating hydroponic system. J. Am. Soc. Hortic. Sci. *123*, 361–364.

58. Ding, G., and Clavero, C. (2017). Silver-Based Low-Emissivity Coating Technology for Energy- Saving Window Applications. In Modern Technologies for Creating the Thin-film Systems and Coatings, N.N. Nikitenkov, ed. (IntechOpen), pp. 409–431.

59. Alonso-Álvarez, D., Ferre Llin, L., Ekins-Daukes, N.J., and Paul, D.J. (2017). ITO and AZO films for low emissivity coatings in hybrid photovoltaic-thermal applications. Sol. Energy *155*, 82–92.

60. Askari, H., Fallah, H., Askari, M., and Mohmmadieyh, M.C. (2014). Electrical and optical properties of ITO thin films prepared by DC magnetron sputtering for low-emitting coatings. arXiv, 1409.5293v1. http://arxiv.org/abs/1409.5293v1.

61. Sims, D.A., and Gamon, J.A. (2002). Relationships between leaf pigment content and spectral reflectance across a wide range of species, leaf structures and developmental stages. Remote Sens. Environ. *81*, 337–354.

62. Price, S.C., Stuart, A.C., Yang, L., Zhou, H., and You, W. (2011). Fluorine substituted conjugated polymer of medium band gap yields 7% efficiency in polymer-fullerene solar cells. J. Am. Chem. Soc. *133*, 4625–4631.

63. Macleod, H.A. (2010). Thin-Film Optical Filters (CRC Press).

64. Bachevillier, S., Yuan, H., Strang, A., Levitsky, A., Frey, G.L., Hafner, A., Bradley, D.D.C., Stavrinou, P.N., and Stingelin, N. (2019). Fully Solution-Processed Photonic Structures from Inorganic/Organic Molecular Hybrid Materials and Commodity Polymers. Adv. Funct. Mater. *29*, 1808152.

65. Tikhonravov, A.V., Trubetskov, M.K., and DeBell, G.W. (2007). Optical coating design approaches based on the needle optimization technique. Appl. Opt. *46*, 704–710.

66. Tikhonravov, A.V., Trubetskov, M.K., and Debell, G.W. (1996). Application of the needle optimization technique to the design of optical coatings. Appl. Opt. *35*, 5493–5508.